

Research Article submitted to Neuroimage

Group-level Spatial Independent Component Analysis of Fourier Envelopes of resting-state MEG data

Pavan Ramkumar¹, Lauri Parkkonen¹, Aapo Hyvärinen²

¹Brain Research Unit, Low Temperature Laboratory, Aalto University School of Science,
PO BOX 15100, 00076 AALTO, FINLAND

²Department of Mathematics and Statistics, Department of Computer Science, University
of Helsinki and Helsinki Institute of Information Technology, Helsinki, FINLAND

Correspondence to: Pavan Ramkumar, Brain Research Unit, Low Temperature
Laboratory, Aalto University School of Science, PO Box 15100, FI-00076 AALTO,
Finland

Email: pavan@neuro.hut.fi, Tel: +358 9 470 28399, Fax: +358 9 470 22969

Key words: Magnetoencephalography, Neural Oscillations, Fourier energy, Independent
Component Analysis, Minimum Norm Estimate, Resting State, Naturalistic Stimulation, Inter-
subject Analysis

Highlights:

- (1) We propose a method to extract narrowband, long-range envelope correlations at the cortical level.
- (2) We apply the method to resting-state MEG data to characterize spontaneous oscillatory networks.
- (3) We interpret these networks by studying their dynamics during naturalistic stimulation.

Manuscript information: 24 text pages, 3 figures, 3 tables

Word Count: 5244 not including references, tables, and figure captions.

Abstract

We developed a data-driven method to spatiotemporally and spectrally characterize the dynamics of brain oscillations in resting-state magnetoencephalography (MEG) data. The method, called envelope spatial Fourier independent component analysis (eSFICA), maximizes the spatial and spectral sparseness of Fourier energies of a cortically constrained source current estimate. We compared this method using a simulated data set against 5 other variants of independent component analysis and found that eSFICA performed best in characterizing dynamics at time scales of the order of minutes.

We then applied eSFICA to real MEG data obtained from 9 subjects during rest. The method identified several networks showing within- and cross-frequency long-range functional connectivity profiles which resemble previously reported resting-state networks, such as the bilateral sensorimotor network at ~ 20 Hz, the lateral and medial parieto-occipital sources at ~ 10 Hz, a subset of the default-mode network at ~ 8 and ~ 15 Hz, and lateralized temporal lobe sources at ~ 8 Hz.

Finally, we interpreted the estimated networks as spatio-spectral filters and applied the filters to obtain the dynamics during a naturalistic stimulus sequence presented to the same 9 subjects. We observed occipital alpha modulation to visual stimuli, bilateral rolandic mu modulation to tactile stimuli and video clips of hands, and the temporal lobe network modulation to speech stimuli, but no modulation of the sources in the default-mode network.

We conclude that (1) the proposed method robustly detects long-range cross-frequency networks at long time scales, (2) the functional relevance of the resting-state networks can be probed by applying the obtained spatio-spectral filters to data from measurements with controlled external stimulation.

1 Introduction

During the past decade, the characterization of resting-state brain networks (RSNs) and their dynamics has become an important field of study (Damoiseaux et al., 2006; Fox and Raichle, 2007). A comprehensive meta-analysis of fMRI studies by Smith et al. (2009) suggests that brain networks active during complex stimulation or task performance were very similar to the networks active during rest. Given that the majority of RSN studies have characterized metabolic variations using positron emission tomography (PET) or hemodynamics using functional magnetic resonance imaging (fMRI), it would certainly be beneficial to characterize RSN dynamics using direct non-invasive measures of neural activity such as electro- or magnetoencephalography (EEG/MEG). One characteristic feature of resting-state networks (RSNs) obtained from fMRI data is that they exhibit long-range correlations in the blood oxygenation level dependent (BOLD) signal. Since BOLD fMRI is a slow and indirect measure of brain activity, electrophysiological equivalents of RSNs using EEG, MEG, or simultaneous EEG and fMRI have been sought (Goldman et al., 2002, Laufs et al., 2003; Mantini et al., 2007; Moosmann et al., 2003). That search has been elusive until recently (dePasquale et al., 2010; Brookes et al., 2011; Knyazev et al., 2011).

Independent component analysis (ICA) is a well established data-driven method for factoring resting-state fMRI data into temporally covarying, spatially independent atoms (Calhoun et al., 2001; Beckmann and Smith, 2005). By contrast, in the analysis of EEG/MEG data, ICA has mainly been applied for artifact rejection. However, as we have argued earlier, ICA is the prime candidate for data-driven characterization of oscillatory activity as measured by EEG/MEG after suitable transformations of the data (Hyvärinen et al., 2010; Ramkumar et al., 2011). In earlier work we have shown that the ICA cost function is more selective to the statistical properties of the oscillatory sources after a sparsifying transform of the data. First, we proposed that applying complex-valued ICA to short-time Fourier transforms (STFTs) of MEG signals is likely to reveal physiologically meaningful components (Hyvärinen et al., 2010). We have referred to this method as Fourier-ICA, but for distinction from other methods here we call it temporal Fourier-ICA (TFICA). Subsequently, we extended complex-valued ICA on STFTs from the sensor space to source space and further argued the advantage of imposing spatial and spectral sparseness on the Fourier coefficients to exploit prior knowledge on the nature of cortical oscillations. We have referred to this method as spatial Fourier-ICA (SFICA) (Ramkumar et al., 2011).

The advantage of TFICA and SFICA, with respect to ordinary ICA on the time-series data (temporal

ICA [TICA] or spatial ICA [SICA]), is that they automatically extract narrowband oscillations from broadband data without having to manually specify a frequency band of interest. However, with TFICA/SFICA we have mainly found components expressing activation in a single region as opposed to connectivity across multiple regions. To specifically address this shortcoming of Fourier-based methods, we hypothesized that the resting-state connectivity is manifest in the envelope correlations between oscillatory dynamics across brain regions.

Accordingly, in this paper, we address two main questions. First, how to robustly characterize electrophysiological resting-state networks using a data-driven method? We propose to apply real-valued TFICA or SFICA on the broadband Fourier spectra (magnitudes of the Fourier coefficients) rather than complex-valued ICA on the complex-valued Fourier coefficients. We call these methods envelope SFICA (eSFICA) or envelope TFICA (eTICA). After benchmarking these envelope methods against the other ICA-based variants on/using? a realistic simulated dataset, we proceed to address the second question: how are MEG resting-state oscillatory networks modulated by stimulation?

2 Materials and methods

2.1 Simulated data

We designed a realistic simulated dataset to test the various ICA-based source separation algorithms using the following methodology. We pre-selected 10 seed regions and placed a current dipole in each of them. The dipoles were oriented normal to the local cortical surface. Source strengths were amplitude-modulated sinusoids at pre-selected carrier frequencies. Table 1 gives a list of these sources along with their MNI coordinates and carrier frequencies. The amplitude-modulated time courses, 2 min in duration and sampled at 150 Hz, were produced as follows.

-----Insert Table 1 here (list of source locations and frequencies) -----

1. The carrier signal was generated by adding uniformly distributed phase noise to a pure sinusoid of a specified frequency (see Table 1). The standard deviation of the phase noise was set to 0.05 times the standard deviation of the sinusoid. Phase noise introduces small jitter and spreads the spectral peak, thus making the signal to better mimic a cortical oscillation.
2. The envelope was generated as follows.
 1. A spike train (simulating e.g. a thalamic pacemaker signal) was modeled as a random binary sequence. We used a temporal sparseness parameter of 0.01 which indicates that 1% of the binary sequence was populated by 1's and the rest by 0's.

2. A basis set of 6 Gaussian functions with an 8-s temporal support was computed. The 6 standard deviations were integral multiples of 0.27 s, ranging up to 1.6 s.
3. The spike train was then convolved with each Gaussian function in the basis, and these convolved signals were added with random weights (loadings of the basis set) constrained to have a unit sum. Together, the sparseness of the spike train and the Gaussian basis parameters determined the temporal sparseness of the envelope.
3. The carrier signal was multiplied by the envelope to generate the amplitude-modulated signal.
4. Pink noise (1/f noise) was added such that the standard deviation of the noise was 10% of that of the amplitude-modulated signal.
5. Finally, the noisy amplitude-modulated signal was constrained to have unit variance.

Thus, each oscillatory source was specified by 14 parameters:

1. Location (orientation perpendicular to the local cortical surface)
2. Carrier frequency of the oscillation
3. Phase-noise variance
4. Temporal sparseness of the spike train
5. The Gaussian basis parameters (basis cardinality, temporal support and spread)
6. The Gaussian basis loadings (weights to combine basis-convolved spike train)
7. Pink-noise level

-----Insert Figure 1 here (all source locations & interactions) -----

Parameters other than location, carrier frequency and the 6 basis loadings remained constant for all 10 sources. The parameters were selected so that a simulated source signal visually resembled a real MEG signal.

Importantly, not all sources were independently generated. Rather, we simulated two types of interactions between sources:

1. Envelope correlation (identical envelope but independent carrier signal)
2. Envelope anticorrelation (inverted envelope and independent carrier signal)

-----Insert Table 2 here (source interactions) -----

The interactions between the sources were symmetric; see Table 2.

After the time series of all the sources were generated as described above, an MEG measurement on the 306-channel Vectorview sensor array (Elekta Oy, Helsinki, Finland) was simulated by computing the corresponding dipolar fields using a single-compartment BEM conductor model with 20480 triangles. Finally, noise was added from a real measurement with a similar sensor array in the absence of a subject at a level of -10 dB with respect to the simulated MEG data..

2.2 Real MEG data

We used the data set presented in our earlier study (Ramkumar et al., 2011). Briefly, we used MEG data obtained with the 306-channel Vectorview system from 9 healthy subjects during 10 minutes of alert resting (eyes open, fixating on a crosshair) and 12 minutes of naturalistic stimulation. The stimuli comprised 6–33 s video clips of faces, hands, and outdoor scenes; recordings of a male voice narrating university history and guitar-playing instructions; short pure tones, and bilateral tactile stimulation to the fingertips. Each stimulus block alternated with a 15-s rest block. Along with MEG, a diagonal electro-oculogram (EOG) was also measured, with one electrode above the left eye and another electrode below the right eye.

2.3 Pre-processing

We pre-processed the data identically as in our earlier work (Ramkumar et al., 2011) with signal space separation (SSS) (Taulu and Kajola, 2005) followed by a custom routine for removing occasional discontinuities (DC jumps) in the data.

2.4 Source localization of short-time Fourier transforms

First, we computed 1-s non-overlapping Hamming-windowed short-time Fourier transforms at the sensor level.

For each subject, the brain's cortical surface was reconstructed from an anatomical MRI using Freesurfer (<http://surfer.nmr.mgh.harvard.edu>, Martinos Center for Biomedical Imaging, Massachusetts General Hospital). We then projected the complex-valued short-time Fourier transformed data to the cortical surface (an average of 5 mm separation between source points for simulated data, and 15 mm for real MEG data) using minimum norm estimation (MNE) followed by depth weighting and noise normalization (often referred to as dynamic statistical parametric

mapping or dSPM; see Dale et al., 2000). We retained only the current estimate in the direction normal to the cortical surface. To avoid the disproportionate emphasis on near-DC fluctuations, we discarded the first 3 Fourier bins corresponding to 0–3.5 Hz before further analysis. In addition to cortical-level STFTs, we also projected the raw sensor-level time series (without computing STFTs) to obtain cortical-level time series.

To avoid sensitivity of the inverse modeling method to the idiosyncrasies of the configuration used to simulate the data, we used a coarser BEM model (5120 triangles) and a source point set excluding exact matches to the simulated source locations to analyze the simulated dataset. Further, for the simulated data, the source localization was performed directly on the canonical Montreal Neurological Institute (MNI) brain. For real MEG data, we first performed the source localization on individual subjects' brains and then projected the cortical-level single-subject data to the MNI brain using a surface-based morphing algorithm (Fischl et al., 1999).

2.5 Blind source separation

Having estimated the space–time–frequency tensor of oscillatory currents at the cortical level, we applied six blind source separation methods to identify functionally distinct networks. After evaluating the results of these methods on the simulated data, we selected the best performing method to apply on real MEG data.

Fourier ICA

Fourier-ICA, as well as the other methods below, was applied in temporal and spatial form. For TFICA and SFICA, we employed the classical noiseless linear mixture model for independent component analysis given by $\mathbf{X} = \mathbf{AS}$, where \mathbf{X} is the complex-valued STFT tensor (time x source points x frequency bins) arranged as a matrix. \mathbf{A} and \mathbf{S} were estimated using the complex-valued FastICA algorithm (Bingham and Hyvärinen, 2000). For TFICA, the tensor was arranged as a matrix of source points x short-time Fourier transforms. ICA on this matrix maximizes independence in the time and frequency domains simultaneously. The rows of the estimated components \mathbf{S} give independent time–frequency atoms, which are then converted into time courses and power spectra by taking the absolute values and averaging over frequency bins and time windows, respectively. The absolute values of the columns of the estimated mixing matrix \mathbf{A} give the spatial maps corresponding to the independent time–frequency atoms. The estimation and interpretation was identical to those in our previous work (Hyvärinen et al., 2010) except that we operated here

at the cortical source rather than at the sensor level. We chose to apply TFICA at the cortical level to facilitate a more direct comparison with other methods. For SFICA, the tensor was rearranged by concatenating the Fourier coefficients for each source point into a row vector for each time window. ICA on this matrix maximizes independence in spatial and frequency domains simultaneously. The estimation and interpretation was exactly as in our previous work (Ramkumar et al., 2011).

Envelope Fourier-ICA

For the envelope-based methods, we applied the same linear mixture model after taking the absolute value of the Fourier coefficients, resulting in $|\mathbf{X}| = \mathbf{A}\mathbf{S}$. The arrangements of the tensor \mathbf{X} for envelope TFICA and envelope SFICA were identical to TFICA and SFICA, respectively.

Ordinary ICA

For comparison, we also applied ordinary ICA, i.e. instead of decomposing the original tensor, we applied temporal and spatial independent component analysis (TICA and SICA) to the spatiotemporal data without going to a Fourier representation.

Once the independent components were estimated, we ranked them by the variance of the columns of the mixing matrix \mathbf{A} .

To reiterate, all the evaluated algorithms comprised two steps: Step 1, a distributed source localization method to obtain cortically-constrained current estimates; Step 2, a variant of independent component analysis (ICA) to separate the sources into oscillatory networks. We investigated the relative merits of 6 variants of ICA: spatial and temporal envelope Fourier ICA, spatial (Ramkumar et al., 2011) and temporal (Hyvärinen et al., 2010) complex-valued Fourier-ICA, and 2 non-Fourier-ICA methods: ordinary spatial and temporal ICA. We compared the performance using 5 different metrics (see Section 2.6). In each case, before applying ICA, we reduced the data to K dimensions ($K = 25$ for the simulated data; $K = 40$ for the real MEG data) using principal component analysis (PCA) followed by whitening.

2.6 Evaluation of algorithms on simulated data

An ideal method would correctly identify the locations of the sources, their power spectra, and their temporal envelopes. It should also capture the interactions between those sources by

grouping sources belonging to one network into the same component. With these general objectives in mind, we focused on temporal and spectral reconstruction, and the effectiveness of network detection. We did not emphasize the accuracy of source localization as much as the effectiveness of network detection because the accuracy of localization is largely dependent on the applied distributed source localization method.

Temporal similarity

For each component, we computed the temporal correlation coefficients between its estimated envelope time course and all true envelopes of the 10 simulated sources. The maximum absolute correlation coefficient was considered to indicate the best matching simulated source. To obtain a concise summary over components, we then took the mean of this maximum absolute correlation to quantify temporal similarity.

Spectral similarity

We computed the power spectrum of all simulated sources (computed as the mean of the non-overlapping 1-s Hamming windowed short-time Fourier transforms). Just as for the temporal similarity metric, for each component, we computed the correlation coefficients between its estimated power spectrum and the true spectra of all 10 simulated sources. The maximum absolute value among these 10 correlation coefficients was considered to indicate the best matching simulated source. As before, we took the mean of this maximum absolute correlation across components to measure the spectral similarity.

Effectiveness of network detection

To compare the ability to identify networks, we first computed a template for each network as follows. We simulated the MEG field produced by each dipolar point source belonging to the network, projected the field back to the cortical surface using a dSPM inverse operator (see Section 2.4), and then summed up all inverse projections of the sources belonging to the given network. Such a template can be treated as a point-spread function of the source, and it factors out the localization errors produced by the distributed inverse modeling method. Thus, any deviation from this template could be attributed to the effects of the empty room measurement noise and the source separation algorithm. We then computed for each of the 4 networks, the spatial correlation between the template map and the spatial map of all estimated independent components. The component with the largest correlation was considered to best represent the

network. This correlation coefficient was treated as a metric of network detection and subsequently compared across the various ICA methods. A larger score indicates a method that better identifies networks.

2.7 Analysis of real MEG data

Based on the results from the simulations (see Section 3.1), we selected eSFICA to be applied on resting-state MEG data and studied the dynamics of the estimated components during naturalistic stimulation. First, we performed the source-localization of the raw time-series data as well as the STFTs using minimum-norm estimation in the same way as in the simulation; see Section 2.4.

Group ICA by two-stage reduction

We applied ICA to a group-level representation of the resting-state MEG data from 9 subjects, obtained by a two-stage reduction (Calhoun et al., 2001). In the first stage, we reduced the data from each subject to 40 dimensions using PCA and whitened them. In the second stage, we temporally concatenated the reduced data from all subjects, and reduced the dimensionality again to 40 using PCA. We then estimated as many components as the dimensionality (i.e. 40) using FastICA.

Selecting consistent components from replicates

We applied ICA as above to resting-state data acquired in a second session from the same 9 subjects. Independent components found to be sufficiently similar in both sessions were retained for further analysis. To set an appropriate threshold for the correlation, we measured this correspondence by a statistical test derived from a specific null hypothesis (Hyvärinen 2011; Hyvärinen and Ramkumar, in preparation). Under this null hypothesis, we assume that the ICA demixing matrix is a random orthogonal matrix; the goal of the statistical test is then to estimate how likely two components correspond across sessions by chance. We set a Bonferroni-corrected false positive rate of $\alpha = 0.05$. Only those components that rejected the null hypothesis were retained for further analysis. For each such component, we computed the correspondence score across sessions as the correlation coefficient between the independent component vectors.

Reconstruction of dynamics during naturalistic stimulation from resting-state spatio-spectral filters

Each independent component estimated from resting-state data can be considered as a linear

“spatospectral” filter, which describes an oscillatory network with a certain spatial pattern of activity. We applied these filters (one for each component) to the short-time Fourier transform of the naturalistic-stimulation data of each subject.

Modulation of amplitude envelope by external stimuli

How do external stimuli modulate networks identified during rest? We addressed this question for each stimulus type, time course (component) and subject, separately as follows. For the 6 different types of stimuli, *viz.* auditory pure tones, natural speech, videos of faces, of hand actions, of natural scenes, and periodic tactile stimuli, we computed the *modulation depth* for each time course given as the percentage signal change from a 15-s epoch preceding the onset of the stimulus block.

We then performed the following second-level analyses on the modulation depths. First, for each component, we performed univariate two-tailed *t*-tests for each stimulus type to determine the modalities for which a component was modulated significantly differently ($p < 0.01$) from zero. Second, to study the specificity of the network to a certain subset of the stimuli, we performed a repeated measures analysis of variance (ANOVA) to assess whether there was a difference in modulation depths across stimulus types. Components that showed a significant difference of modulation depth ($p < 0.05$) between stimulus types were labeled “Specific”.

Testing for eye-movement artifacts

To test the possibility that some components were related to eye-movement artifacts, we computed correlations between the absolute value of the electro-oculogram (EOG) with the time course of each component obtained by applying the spatiospectral filter to the naturalistic stimulation data (after downsampling to 1 Hz), separately for each subject. For each component, we performed a univariate two-tailed *t*-test to examine whether its `time_course` was statistically significantly ($p < 0.05$) correlated with the EOG envelope (absolute value of the `time_course`).

Visualization

Each independent component represents a spatiospectral filter, i.e. the set of Fourier powers concatenated across source points. We computed the spatial profile (map) by averaging the independent component across the Fourier bins for each source point. The spatial maps were thresholded at the 95th percentile. We computed the positive and negative spectral profiles by

averaging the independent component across source points exceeding the 95th percentile threshold in positive and negative directions respectively. Although the independent components were calculated from 3.5–75 Hz, the power spectra were only visualized from 3.5–40 Hz because the spectra had extremely small values in the range 40–70 Hz. Finally, we plotted the modulation depths for each stimulus modality as bars, along with error bars representing the standard errors of mean (SEM) across the 9 subjects.

3 Results

3.1 Results on simulated data

Table 3 shows the metrics for temporal and spectral similarity and the 4 network detection metrics for the 6 different ICA algorithms. Among the two envelope methods, eSFICA performs much better in temporal and spectral reconstruction, whereas eTFICA performs slightly better in network detection.

----Insert Table 3 here (comparison of methods by metrics)----

3.2 Results on real MEG data

Figures 2 and 3 show the estimated resting-state components: their spatial and spectral profiles, as well as their modulation by naturalistic stimuli. Based on the modulation depths and the spatial profiles, we manually rearranged the components into sensorimotor, medial visual, lateral visual, auditory, higher-order sensorimotor, intrinsic, and orbitofrontal components. The grouping is only approximative, and could be contested for several components. However, instead of creating a 'miscellaneous' category for such components, we prefer to assign each component to the closest cluster. In the following, we make some remarks about the components.

----Insert Figures 2-3 here (list of all RSNs)----

Sensorimotor components

We found two unilateral ~10-Hz, two unilateral ~15-Hz, and one bilateral ~20-Hz sensorimotor components (Figure 2, top panel) spanning the primary somatosensory and motor cortices, as well as the supplementary motor areas (SMA): these were statistically significantly modulated by tactile stimuli alone.

Medial visual components

We observed one bilateral and two lateralized medial parieto-occipital components at ~10 Hz (see Figure 2, middle panel). These were modulated non-specifically by speech, faces, hands, scenes, and tactile stimuli. The bilateral component peaked slightly below 10 Hz, whereas the lateralized components peaked slightly above 10 Hz.

Lateral visual components

We also observed several components at ~8–15 Hz with spatial maxima over the ventral temporo-occipital pathways (Figure 2, bottom panel). Most of these components were individually modulated by at least one visual stimulus category. Hence we classified them as higher-order visual components.

Auditory components

We found one ~8-Hz component with bilateral maxima in the auditory cortices, but this component was modulated by speech, faces and hands. In addition, we found two ~15-Hz components with spatial maxima in the left and right auditory cortex and superior temporal cortex, which were modulated by speech and tactile stimuli (see Figure 3, top panel). The left hemisphere component was also significantly correlated ($p < 0.05$; $r = 0.14$; mean across subjects) with the EOG envelope.

Higher-order sensorimotor components

We found several ~12–20-Hz components with local maxima in the primary and secondary sensorimotor areas, and posterior parietal cortices (Figure 3, second panel). However, unlike the sensorimotor components that were modulated only by tactile stimuli, these components were modulated non-specifically by speech, faces, hands, places, and tactile stimuli.

Intrinsic components

We found two lower-frequency (< 5 Hz) components with spatial maxima in the posterior cingulate, mid-cingulate and parts of the orbitofrontal cortex (Figure 3, third panel). We found another low-frequency component in the right anterior inferior temporal cortex that was not significantly modulated by any stimulus category. We classified all these components as intrinsic because they exhibit either weak or no modulation to external stimuli. However, the first and the third intrinsic components were weakly but significantly ($p < 0.05$) correlated with the EOG

envelopes ($r = 0.08$ and 0.06 respectively; mean across subjects).

Orbitofrontal components

We found three components with large spatial maxima in the orbitofrontal cortices alone (Figure 3, bottom panel). Two of these three components showed the largest envelope correlation ($r = 0.17$ and 0.15 , respectively; mean across subjects) with the absolute value of the EOG envelopes, and the correlations were statistically significantly ($p < 0.05$) different from zero.

4 Discussion

4.1 Comparison of the algorithms

From the performance metrics of the various algorithms, some clear patterns emerge. First, the spatial Fourier methods seem to be better at estimating the temporal profiles of the sources, whereas the temporal Fourier methods excel at identifying the corresponding networks. This observation implies that the mixing matrices are more accurately estimated than the independent components, suggesting the added value of applying both spatial and temporal source separation methods. It is possible that a hybrid spatiotemporal method, e.g. the one proposed by Stone et al. (2002) for fMRI data, would be able to combine the advantages of both types of methods. The non-Fourier-based methods (SICA and TICA) are poor at estimating networks. The observation could be explained by the fact that these methods impose either temporal or spatial sparseness, whereas most networks seem to exhibit narrowband oscillations and would thus benefit from an imposition of spectral sparseness.

4.2 Identified resting-state networks

Our results demonstrated the ~ 10 - and ~ 20 -Hz components of the rolandic sensorimotor mu rhythm (Hari and Salmelin, 1997). Robust inter-hemispheric correlations in the sensorimotor network have been observed in fMRI (Biswal et al., 1995) and in intracranial recordings (Nir et al., 2008). It is interesting to note that the ~ 20 -Hz component, but not the ~ 10 -Hz components, showed a bilateral spatial profile. Early MEG studies indicate that the ~ 20 -Hz oscillation is generated precentrally and appears more related to motor than somatosensory processing whereas the ~ 10 -Hz oscillation is postcentral and associated with processing of tactile information, although both rhythms are modulated by movement and tactile stimulation (for a review see Hari and Salmelin, 1997). Thus, understanding the inter-hemispheric coupling of these two spontaneous rhythms would be useful in further elucidating their role in sensorimotor processing.

The bilateral medial parieto-occipital component was modulated by speech and visual stimuli but not by tactile stimuli, whereas the unilateral component was modulated by tactile stimuli as well. The spatial maxima correspond to previously reported generators of the classical ~10-Hz parieto-occipital alpha rhythm. Most of the identified higher-order visual components in the 8–15-Hz range had the sources in the right lateral temporal lobe.

The bilateral auditory component showed a peak at ~8 Hz which corresponds to the tau rhythm reported in an early MEG study (Tiihonen et al., 1991). In addition to speech, this component was modulated by videos of faces and hands as well. The left and right lateralized temporal lobe components were modulated by speech and tactile stimuli at ~12 Hz. Spontaneous rhythms in the auditory cortex and speech production areas have been linked to speech production and perception networks along with frequency-specific lateralization (Giraud et al., 2007). However, we did observe any differences in the power spectra between the left and right hemisphere components.

The higher-order sensorimotor components showed peaks at ~10 and ~20 Hz, and were modulated not only by tactile stimuli, but also by visual and speech stimuli. Given that the video clips contained pictures of faces and hand actions, and some speech segments described instructions for guitar fingering, the sensorimotor suppression to these stimulus categories is not unexpected.

Among the intrinsic components, the second and third (at low frequencies) are slightly lateralized and appear to represent the fronto-parietal attention networks. Unlike Brookes et al. (2011), we did not find components describing the entire default mode network. We also could not find the cerebellar network that Brookes et al. (2011) identified because we defined our source points on the cortical surface alone.

The putative orbitofrontal components seem to be related to eye-movement artifacts. This finding is not surprising considering that earlier studies have localized eye-blink artifacts to the orbit (Antervo et al., 1985). Although the correlations between EOG signal envelopes and the component envelope time courses are low, and the variance of the entire component cannot be explained by the EOG signals alone, caution must be exercised while interpreting these components as brain activity.

4.2 Methodological strengths and caveats

Advantages of eSFICA

First, while TFICA or SFICA are devised to reveal long-range phase synchrony, we did not find such components when applying these methods to either simulated or real data (Hyvärinen et al., 2010; Ramkumar et al., 2011). One possible explanation is that phase synchrony was only intermittent and thus was not robustly detectable with exploratory methods over time scales of minutes. Indeed, analysis in earlier studies reporting long-range phase-synchrony has typically been carried out trial by trial and over a time scale of hundreds of milliseconds to a few seconds (see e.g. Palva et al., 2009; Palva et al., 2010).

By contrast, eSFICA was able to find components with spatial maps showing bilateral networks such as the sensorimotor network, and a subset of the default mode network. Due to the real-valued nature of the method, the captured interactions are envelope correlations and they disregard phase interactions. Second, since the ICs are zero-mean, it is possible to find envelope anti-correlations using this method. Third, compared with the method applied by Brookes et al. (2011), our method is automatically able to select relevant narrow frequency bands in a data-driven manner. As a result, the method can potentially find cross-frequency interactions within a single network.

Potential biases to the simulated data

Although we designed the simulated data set to closely mimic real MEG data, some artificial biases may still be present. For instance, increasing the temporal sparseness of the source time courses favors temporal ICA methods. To reduce this possible bias, we adjusted the temporal sparseness parameter so that the simulated time courses visually resembled real MEG data.

Potential weaknesses in the group analysis

In this paper, we have adopted the standard approach of temporal concatenation across subjects (Calhoun et al., 2001; Beckmann and Smith, 2005). However, individual application of ICA on single-subject data, followed by post-hoc testing of consistency (Esposito et al., 2005; Langers, 2010; Hyvärinen, 2011) would make fewer assumptions on the similarity of statistical properties of the data from different subjects. Optimizing the group analysis is certainly an avenue for future methodological development.

5 Conclusion

We developed a data-driven method to characterize resting-state oscillatory brain networks at the cortical level across subjects. The identified RSNs were in agreement with those previously reported in the fMRI and MEG literature. Further, we showed that a majority of these RSNs were consistently modulated by external stimulation, while the ‘intrinsic’ networks remained seemingly unaffected by stimulation.

6 Acknowledgements

This study was supported by the Finnish Graduate School of Neuroscience, ERC (Advanced Grant #232946 to R. Hari), the Academy of Finland (Finnish Centre of Excellence Program 2006–2011) and the aivoAALTO project of Aalto University. We thank Riitta Hari for valuable comments on the manuscript.

7 References

- Abou-Elseoud, A., Starck, T., Remes, J., Nikkinen, J., Tervonen, O., Kiviniemi, V., 2010. The effect of model order selection in group PICA. *Hum Brain Mapp* 31, 1207–1216.
- Antervo, A., Hari, R., Katila, T., Ryhänen, T., Seppänen, M., 1985. Magnetic fields produced by eye-blinking. *Electroenceph Clin Neurophysiol* 61, 247–253.
- Beckmann, C.F., Smith, S.M., 2005. Tensorial extensions of independent component analysis for multisubject fMRI analysis. *Neuroimage* 25, 294–311.
- Biswal, B., Yetkin, F.Z., Haughton, V.M., Hyde, J.S., 1995. Functional connectivity in the motor cortex of resting human brain using echo-planar MRI. *Magn Reson Med* 34, 537–541.
- Brookes, M.J., Woolrich, M., Price, D., Hale, J.R., Stephenson, M.C., Barnes, G.R., Smith, S.M., Morris, P.G., 2011. Investigating the electrophysiological basis of resting-state networks using magnetoencephalography. *Proc Natl Acad Sci USA* 108, 16783–16788.
- Calhoun, V.D., Adali, T., Pearlson, G.D., Pekar, J.J., 2001. A method for making group inferences from functional MRI data using independent component analysis. *Hum Brain Mapp* 14, 140–151.
- Damoiseaux J.S., Rombouts, S.A.R.B., Barkhof, F., Scheltens, P., Stam, C.J., Smith, S.M., Beckmann, C.F., 2006. Consistent resting-state networks across healthy subjects. *Proc Natl Acad Sci USA* 103, 13848–13853.
- de Pasquale, F., Penna, S.D., Snyder, A.Z., Lewis, C., Mantini, D., Marzetti, L., Belardinelli, P., Ciancetta, L., Pizzella, V., Romani, G.L., Corbetta, M., 2010. Temporal dynamics of spontaneous MEG activity in brain networks. *Proc Natl Acad Sci USA* 107, 6040–6045.
- Esposito, F., Scarabino, T., Hyvärinen, A., Himberg, J., Formisano, E., Comani, S., Tedeschi, G.,

Goebel, R., Seifritz, E., Di Salle, F., 2005. Independent component analysis of fMRI group studies by self-organizing clustering. *Neuroimage* 25, 193–205.

Fox M.D., Raichle, M.E., 2005. Consistent resting-state networks across healthy subjects. Spontaneous fluctuations in the brain observed with functional magnetic resonance imaging. *Nat Rev Neurosci* 8, 700–711.

Fischl, B., Sereno, M.I., Tootell, R.B., Dale, A.M. 1999. High-resolution intersubject averaging and a coordinate system for the cortical surface. *Hum Brain Mapp* 8, 272–284.

Giraud, A.L., Kleinschmidt, A., Poeppel, D., Lund, T.E., Frackowiak, R., and Laufs, H., 2007. Endogeneous cortical rhythms determine hemispheric dominance for speech. *Neuron* 56, 1127–1134.

Goldman, R.I., Stern, J.M., Engel Jr., J., Cohen, M.S., 2002. Simultaneous EEG and fMRI of the alpha rhythm. *Neuroreport* 13, 2487–2492.

Hari, R., Salmelin, R., 1997. Human cortical oscillations: a view through the skull. *Trends Neurosci* 20, 44–49.

Hyvärinen, A., Ramkumar, P., Parkkonen, L., Hari, R., 2010. Independent component analysis of short-time Fourier transforms for spontaneous EEG/MEG analysis. *Neuroimage* 49, 257–271.

Hyvärinen, A., 2011. Testing the ICA mixing matrix based on inter-subject or inter-session consistency. *Neuroimage* 58, 132–136.

Hyvärinen, A., Ramkumar, P., 2011. Testing independent components by inter-subject or inter-session consistency (In Preparation).

Knyazev, G.G., Slobodskoj-Plusnin, J.Y., Bocharov, A.V., Pylkova, L.V., 2011. The default mode network and EEG alpha oscillations: An independent component analysis. *Brain Res* 1402, 67–69.

Langers, D.R.M., 2010. Unbiased group-level statistical assessment of independent component maps by means of automated retrospective matching. *Hum Brain Mapp* 31, 727–742.

Laufs, H., Krakow, K., Sterzer, P., Eger, E., Beyerle, A., Salek-Haddadi, A., Kleinschmidt, A., 2003. Electroencephalographic signatures of attentional and cognitive default modes in spontaneous brain activity at rest. *Proc Natl Acad Sci USA* 100, 11053–11058.

Mantini, D., Perrucci, M.G., Del Gratta, C., Romani, G.L., Corbetta, M., 2007. Electrophysiological signatures of resting state networks in the human brain. *Proc Natl Acad Sci USA* 104, 13170–13175.

Moosmann, M., Ritter, P., Krastel, I., Brink, A., Thees, S., Blankenburg, F., Taskin, B., Obrig, H., Villringer, A., 2003. Correlates of the alpha rhythm in functional magnetic resonance imaging and near infrared spectroscopy. *Neuroimage* 20, 145–158.

Nir, Y., Mukamel, R., Dinstein, I., Privman, E., Harel, M., Fisch, L., Gelbard-Sagiv, H., Kipervasser, S., Andelman, F., Neufeld, M.Y., Kramer, U., Arieli, A., Fried, I., Malach, R., 2008. Interhemispheric correlations of slow spontaneous neuronal fluctuations revealed in human sensory cortex. *Nat*

Neurosci 11, 1100–1108.

Palva, S., Monto, S., Palva, J.M., 2009. Graph properties of synchronized cortical networks during visual working memory maintenance. *Neuroimage* 49, 3257–3268.

Palva, J.M., Monto, S., Kulashekhar, S., Palva, S., 2010. Neuronal synchrony reveals working memory networks and predicts individual memory capacity. *Proc Natl Acad Sci USA* 107, 7580–7585.

Ramkumar, P., Parkkonen, L., Hari, R., Hyvärinen, A., 2011. Characterization of neuromagnetic brain rhythms over time scales of minutes using spatial independent component analysis. *Hum Brain Mapp*, Epub Ahead of Print.

Smith, S.M., Fox, P.T., Miller, K.L., Glahn, D.C., Fox, P.M., Mackay, C.E., Filippini, N., Watkins, K.E., Toro, R., Laird, A.R., Beckmann, C.F., 2009. Correspondence of the brain's functional architecture during activation and rest. *Proc Natl Acad Sci USA* 106, 13040–13045.

Stone, J.V., Porrill, J., Porter, N.R., Wilkinson, I.D., 2002. Spatiotemporal independent component analysis of event-related fMRI data using skewed probability density functions. *Neuroimage* 15, 407–421.

Taulu, S., Kajola, M., 2005. Presentation of electromagnetic multichannel data: The signal space separation method. *J Appl Phys* 97, 124905–124910.

Tiihonen, J., Hari, R., Kajola, M., Karhu, J., Ahlfors, S., Tissari, S., 1991. Magnetoencephalographic 10-Hz rhythm from the human auditory cortex. *Neurosci Lett* 129, 303–305.

8 Figure Captions

Figure 1. Top: Locations of the simulated oscillatory current sources on an inflated and flattened brain surface. Bottom: Envelopes and power spectra of each source. Sources 1–4 constitute network #1, source 5 network #2, sources 6–8 network #3, and sources 9–10 network #4.

Figure 2. First 3 component groups: eSFICA spatio-spectral filters obtained from resting-state data (left and middle panels) used to interrogate brain dynamics during natural stimulation (right panel). Left: The spatial profiles obtained by averaging the independent component across the Fourier bins. The maps are thresholded at the 95th percentile. Middle: The (positive and negative) spectral profiles are obtained by averaging the independent component across source points exceeding the 95th percentile threshold in positive and negative directions, respectively. The inset shows consistency of the spatio-spectral filter across two resting-state sessions as measured by Pearson's correlation coefficient. Right: The temporal profile is described by the modulation depths for each stimulus category averaged across subjects. Error bars show standard errors of mean. A star indicates that the component is modulated significantly differently ($p < 0.05$; uncorrected) from zero. The label "Specific" suggests that there are statistically significant differences ($p < 0.05$) between effect sizes of different stimulus categories. We manually ordered the components according to the dominant modality as sensorimotor, medial visual and lateral visual components.

Figure 3. Subsequent 4 component groups: eSFICA spatio-spectral filters obtained from resting-state data (left and middle panels) used to interrogate brain dynamics during natural stimulation (right panel). Left: The spatial profiles obtained by averaging the independent component across the Fourier bins. The maps are thresholded at the 95th percentile. Middle: The (positive and negative) spectral profiles are obtained by averaging the independent component across source points exceeding the 95th percentile threshold in positive and negative directions, respectively. The inset shows consistency of the spatio-spectral filter across two resting-state sessions as measured by Pearson's correlation coefficient. Right: The temporal profile is described by the modulation depths for each stimulus category averaged across subjects. Error bars show standard errors of mean. A star indicates that the component is modulated significantly differently ($p < 0.05$; uncorrected) from zero. The label "Specific" suggests that there are statistically significant differences ($p < 0.05$) between the effect sizes of different stimulus categories. We manually ordered the components as auditory, higher-order sensorimotor, intrinsic components and artifacts.

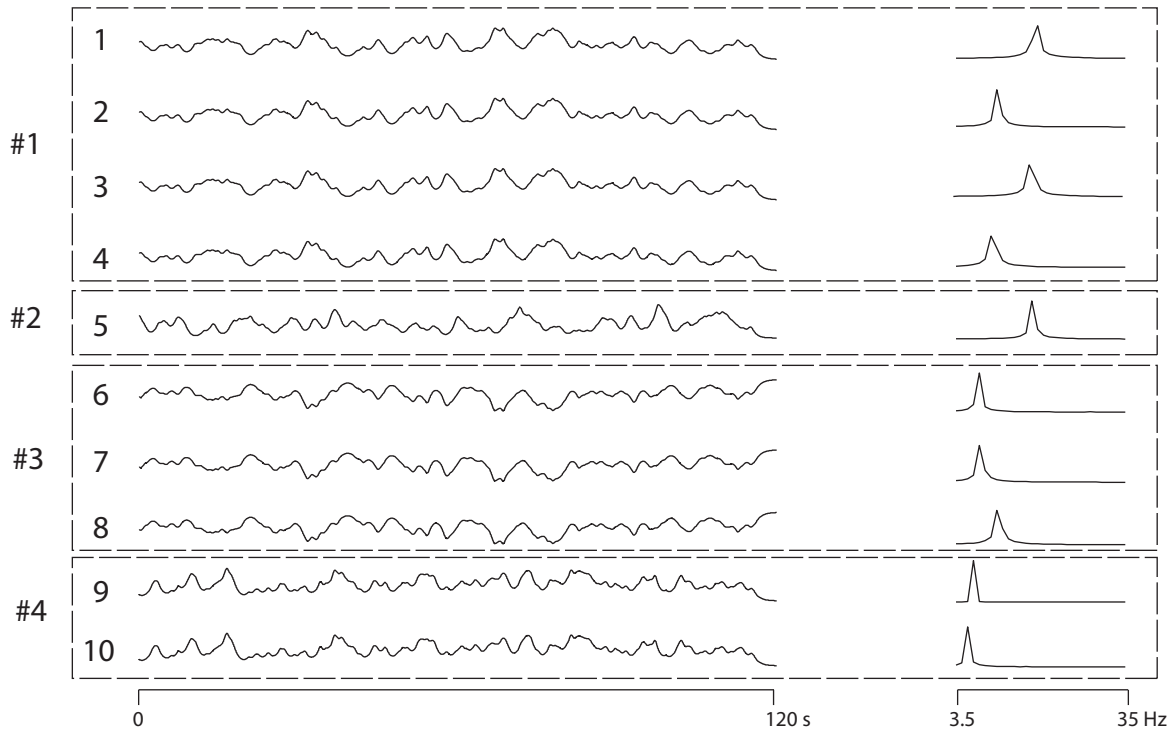
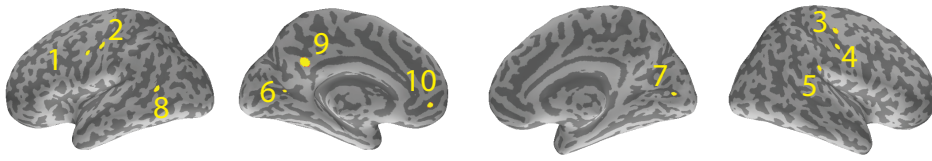
9 Tables

Table 1: Simulated sources. Regions, Montreal Neurological Institute (MNI) co-ordinates and carrier frequencies.

Source index	Region	MNI Coordinates (x y z) (mm)	Frequency (Hz)
1	Left central sulcus (MI)	-53.2 3.4 35.2	19.5
2	Left central sulcus (SI)	-46.5 13.3 41.9	12.0
3	Right central sulcus (MI)	40.7 -16.9 55.5	19.2
4	Right central sulcus (SI)	49.3 -17.2 37.0	11.0
5	Right posterior parietal operculum (SII)	58.0 -35.4 28.4	19.0
6	Left calcarine sulcus	-25.9 -71.8 7.4	8.0
7	Right calcarine sulcus	12.4 -89.7 4.0	8.5
8	Left lateral middle temporal area (MT)	-42.9 -52.7 5.4	12.1
9	Left posterior cingulate cortex (PCC)	-5.5 -48.1 30.1	7.0
10	Left medial prefrontal cortex (MPFC)	-41.5 69.0 64.6	6.0

Table 3: Comparison of the six source separation algorithms. Each column represents one method. The rows the metric describing the overall temporal similarity, overall spectral similarity, and the detectability of an individual network (see Section 2.6 in the text for details). The best performing algorithm for each criterion is highlighted. The last two rows give the mean of network detectability and the grand mean score across all metrics.

	Spatial			Temporal		
Metric	eSFICA	SFICA	SICA	eTFICA	TFICA	TICA
Temporal similarity	0.50	0.50	0.56	0.15	0.32	0.30
Spectral similarity	0.47	0.76	0.79	0.20	0.68	0.52
Detection of network 1	0.74	0.60	0.03	0.76	0.67	0.03
Detection of network 2	0.67	0.49	0.03	0.81	0.67	0.03
Detection of network 3	0.75	0.45	0.04	0.77	0.35	0.03
Detection of network 4	0.75	0.49	0.02	0.71	0.67	0.02
Detection of networks (mean)	0.73	0.51	0.03	0.77	0.59	0.03
Grand Mean Score	0.60	0.59	0.46	0.37	0.53	0.29

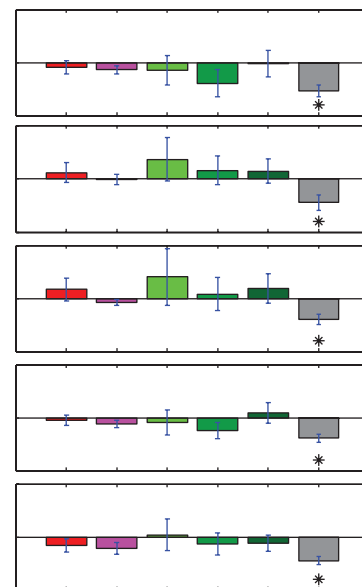
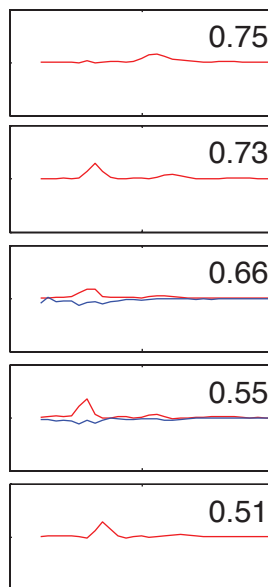
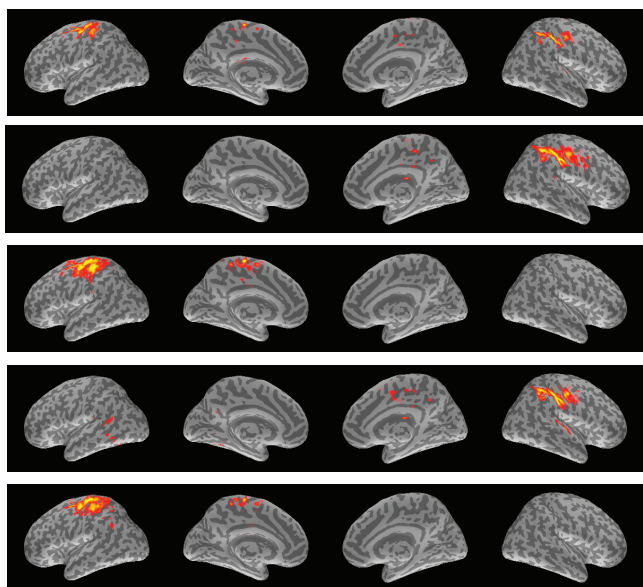


Spatial Profile

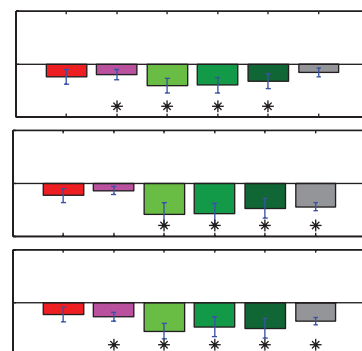
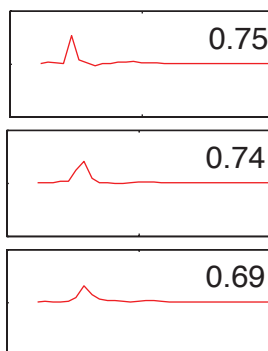
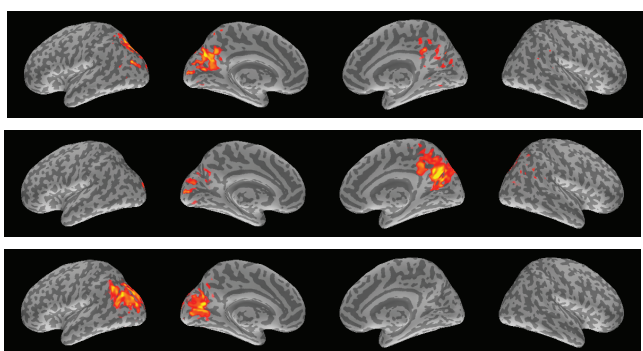
Spectral Profile

Temporal Profile

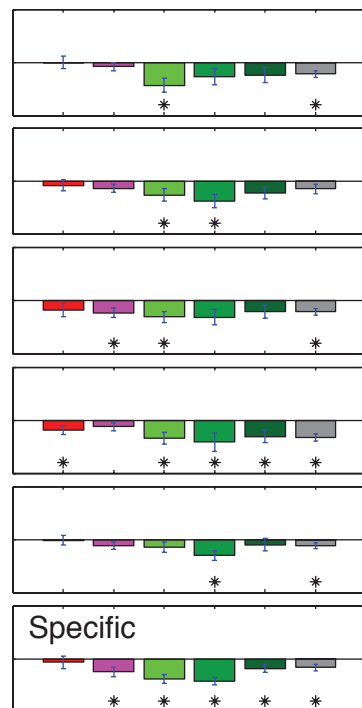
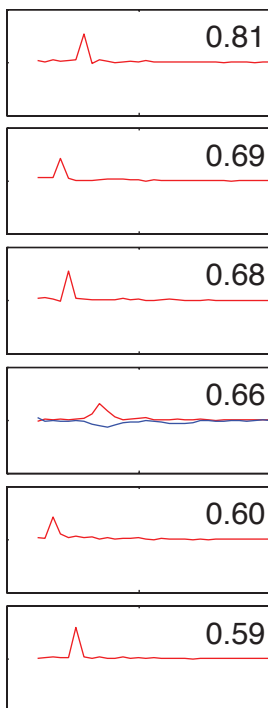
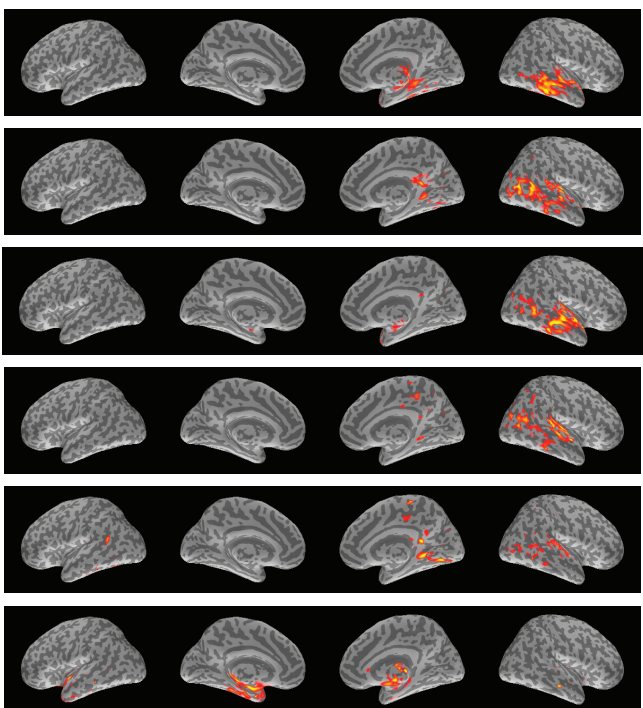
Sensorimotor



Medial Visual



Lateral Visual



Beeps Speech Faces Hands

0 10 20 30 40 Hz

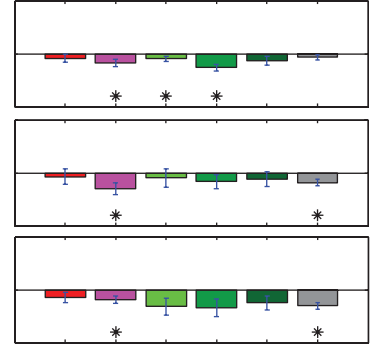
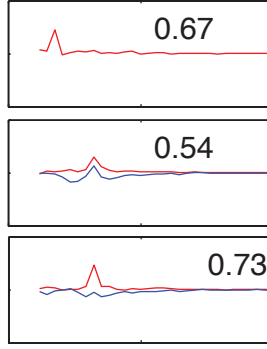
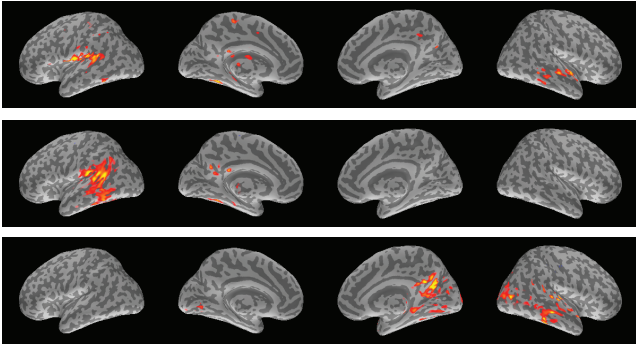
Places Tactile

Spatial Profile

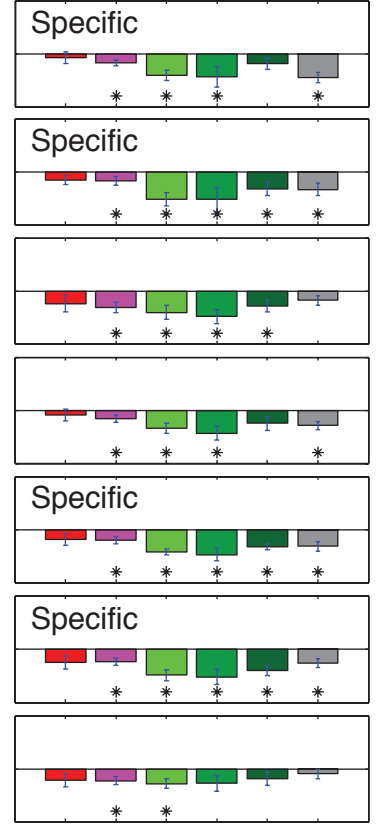
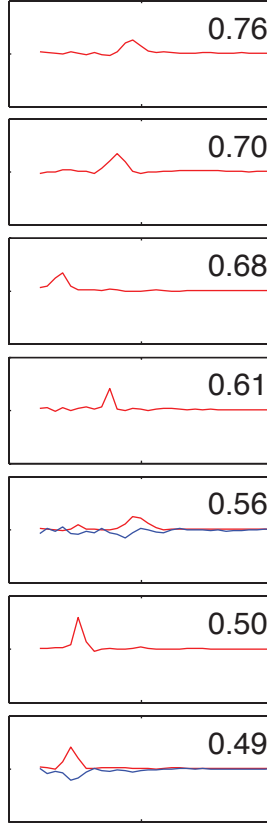
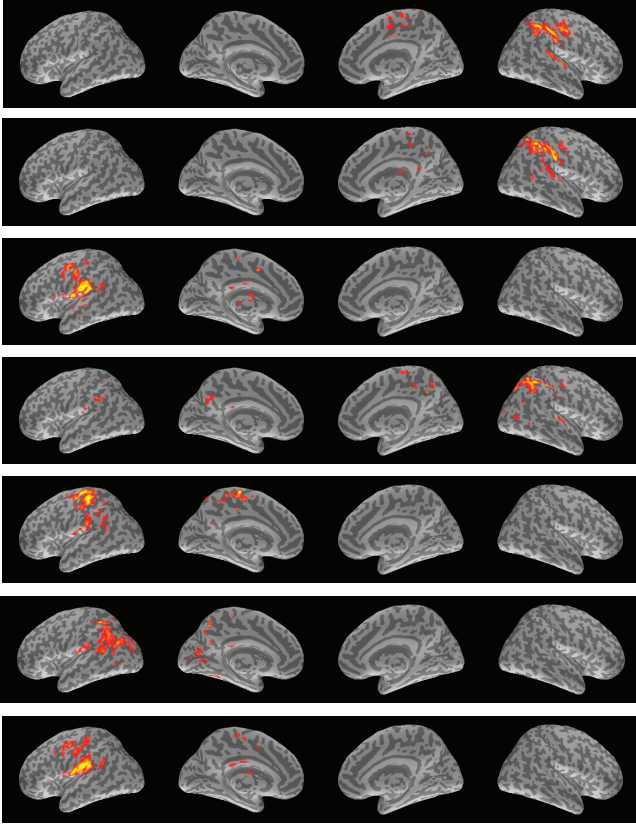
Spectral Profile

Temporal Profile

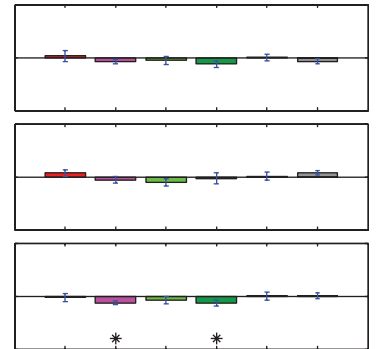
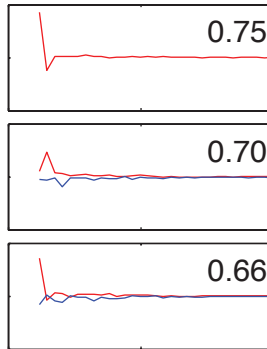
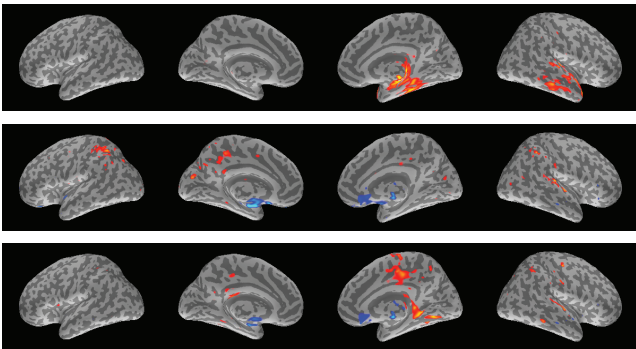
Auditory



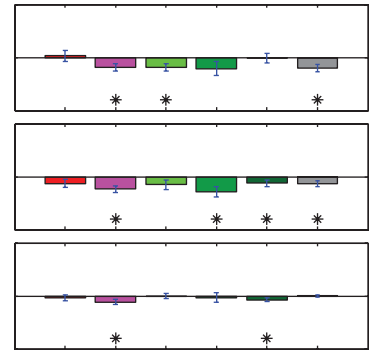
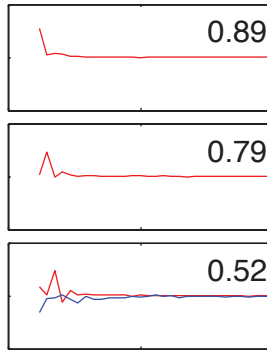
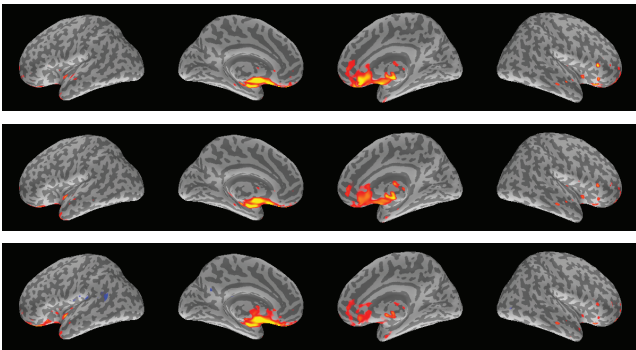
Higher-order sensorimotor



Intrinsic



Artifactual



Beeps Speech Faces Hands

0 10 20 30 40 Hz

Places Tactile